THE 1983 JUNE 15 OCCULTATION BY NEPTUNE. II. THE OBLATENESS OF NEPTUNE

RICHARD G. FRENCH, PAMELA A. MELROY,[a] RICHARD L. BARON, EDWARD W. DUNHAM, KAREN J. MEECH,[b] AND DOUGLAS J. MINK[c]
Department of Earth, Atmospheric, and Planetary Sciences, Massachusetts Institute of Technology, Cambridge, Massachusetts 02139

J. L. ELLIOT
Department of Earth, Atmospheric, and Planetary Sciences, and Department of Physics, Massachusetts Institute of Technology, Cambridge, Massachusetts 02139

DAVID A. ALLEN
Anglo-Australian Observatory, P. O. Box 296, Epping, New South Wales, 2121, Australia

MICHAEL C. B. ASHLEY AND KENNETH C. FREEMAN
Mount Stromlo Observatory, Private Bag, Woden P. O., Canberra, ACT 2606, Australia

EDWIN F. ERICKSON
Ames Research Center, Moffett Field, Mountain View, California 94035

JAY GOGUEN AND H. B. HAMMEL
Institute for Astronomy, University of Hawaii, 2680 Woodlawn Drive, Honolulu, Hawaii 96822
Received 17 May 1985; revised 20 August 1985

ABSTRACT

The oblateness and radius of Neptune were determined from an analysis of photoelectric observations of the 15 June 1983 occultation by Neptune at six stations, combined with the results of the 7 April 1968 Neptune occultation of BD − 17°4388. The oblateness is 0.0191 ± 0.0017 and the equatorial radius is $25\,268 \pm 12$ km at the level probed by the occultation. The results are consistent with recent determinations of Neptune's rotation period and J_2 (the second-order gravitational harmonic coefficient) and suggest that Neptune is far less centrally condensed than Uranus. Temperature profiles for Neptune's upper atmosphere were also derived from these data.

I. INTRODUCTION

On 15 June 1983, Neptune occulted MKE 30, one of the events listed by Mink *et al.* (1981). The event was successfully observed from several stations, and the favorable occultation geometry made possible a sensitive search for ring material around Neptune. In a companion paper (Elliot *et al.* 1985), we describe the results of such a ring search, using observations made from the *Kuiper Airborne Observatory* (*KAO*), Mount Stromlo Observatory (MSO), the Anglo-Australian Telescope (AAT) and the ANU 1.0 m telescope at Siding Spring, the Infrared Telescope Facility (IRTF), and the University of Hawaii 2.2 m telescope (UH). Here, we use these observations to determine the size and oblateness of Neptune, and to obtain temperature profiles of Neptune's upper atmosphere.

In the next section, we describe the observations briefly; a more detailed description is given by Elliot *et al.* (1985). In Sec. III, we describe the event astrometry and combine our observations with occultation results from the 7 April 1968 occultation by Neptune of BD − 17°4388 to determine Neptune's size and oblateness. We present upper atmospheric temperature profiles obtained from the 1983 observations. In Sec. IV, we discuss the physical implications of our results, and compare our findings to Hubbard *et al.*'s (1985) analysis of independent observations of the 15 June 1983 event. Finally, in Sec. V, we present our conclusions.

[a] Current affiliation: United States Air Force.
[b] Guest Observer, Infrared Telescope Facility.
[c] Current affiliation: Harvard-Smithsonian Center for Astrophysics, 60 Garden Street, Cambridge, MA 02138.

II. OBSERVATIONS

We obtained useful observations of the 15 June 1983 occultation from six telescopes of meter class: *KAO*, MSO, AAT, ANU, IRTF, and UH. The observational circumstances, the equipment used, and the means of recording the data and timing information at each station are discussed in the companion paper by Elliot *et al.* (1985). For convenient reference, Table I lists the telescope apertures and filter characteristics for each of the six stations.

TABLE I. 15 June 1983 observations.

Station	Telescope Aperture (m)	λ (μm)	Δλ (μm)	Notes
KAO	0.9	0.50	0.07	Emersion only
		0.73	0.09	Emersion only
		0.78	0.20	Immersion only
		0.83	0.07	Emersion only
		2.2	0.4	
MSO	1.9	0.55	0.10	
		0.85	0.10	
AAT	3.9	2.2	0.4	
ANU	1.0	0.55	0.10	
		0.85	0.10	
IRTF	3.0	2.2	0.4	
UH	2.2	0.86	0.08	

0004-6256/85/122624-15$00.90

a) 15 June 1983 Event Timing

Accurate measurements of the times of immersion and emersion of the occulted star correspond to points along the planetary limb as viewed from the Earth. The oblateness and radius of the planet can be determined by matching the observations with a model limb profile for an oblate planet. Using this method, stellar occultation observations have been widely used to determine the oblateness of planetary upper atmospheres (cf. Table 2a of Elliot 1979, and references cited therein; Elliot *et al.* 1980; Elliot *et al.* 1981; and French and Taylor 1981). Since the limb of a planet is not sharp, immersion and emersion occur gradually, and a choice must be made concerning the definition of the planetary limb. For our present analysis, we obtained occultation times for immersion and emersion by fitting a model isothermal light curve to each observation. Four free parameters were determined: the half-light time $t_{1/2}$, the mean atmospheric scale height H, and the zero- and full-intensity levels. Ideally, one would like to determine occultation times corresponding to points lying on a constant-potential surface, but in practice this has been difficult to achieve. Melroy (1984) discusses a method of determining points on an isobaric surface by inverting the observations to determine atmospheric pressure as a function of time along the light curve.

Since all the observed light curves contain sharp spikes caused by Neptune's atmosphere, they differ significantly from the model isothermal curves, and the formal uncertainty in the half-light time given by the least-squares fit is not an accurate measure of true uncertainty. In practice, the fitted value for the half-light time depends on the interval of the light curve used in the isothermal fit. This can be attributed primarily to uncertainties in the zero- and full-intensity levels. Based on a series of fits using different amounts of data, we find that the half-light time uncertainty varies roughly as

$$\sigma_\epsilon(t_{1/2}) \cong 11.1(H/v_\perp)^{1/2}\epsilon, \tag{1}$$

where $v_\perp$ is the component of the event velocity perpendicular to the planetary limb and ϵ is a measure of the noise present in a light curve over an integration of 1 s, normalized by the full stellar intensity (see French *et al.* 1978). (We note that this is substantially larger than the theoretical value of $\sigma(t_{1/2}) = 3.55\,(H/v_\perp)^{1/2}\,\epsilon$ found by French *et al.* (1978) for a noisy *isothermal* light curve whose zero- and full-intensity levels were *known perfectly*, rather than being determined from the fit).

True variations in the mean scale height from one suboccultation point to another are another important source of error. If the mean scale height has a typical variation of ΔH between suboccultation points, then the half-light rays will suffer variations in transverse deflection of ΔH by the time they reach the Earth, due to refraction by Neptune's atmosphere. This can be regarded as an additional uncertainty in the half-light time, given by

$$\sigma_{\Delta H}(t_{1/2}) = \Delta H/v_\perp. \tag{2}$$

Adopting $\Delta H = 6$ km, as determined from the range of mean scale heights obtained from our isothermal fits, and using $v_\perp \simeq 22$ km s^{-1}, a typical value for the 1983 occultation, we find $\sigma_{\Delta H}(t_{1/2}) \simeq 0.27$ s. Combining Eqs. (1) and (2) in quadrature, we adopt

$$\sigma(t_{1/2}) = [\sigma^2_{\Delta H}(t_{1/2}) + \sigma^2_\epsilon(t_{1/2})]^{1/2} \tag{3}$$

as a measure of the timing uncertainty of our observations.

We determined half-light times for all of our observations, using the methods described above, with the results presented in Table II. Except as noted, isothermal fits were performed to 200 s of data, from 60 s above half light to 140 s below half light. Also included is the quantity $(v_\perp/H)^{1/2}\epsilon$, a nondimensional measure of the noise level of an occultation, allowing direct comparison with other occultations. Details of the analysis for each station are discussed below.

1) KAO

Immersion was observed in two channels and emersion was observed in four channels. Figures 1 and 2 show the summed light curves for immersion and emersion, respec-

TABLE II. Event times and mean temperatures for 15 June 1983 observations.

Station	Latitude	Longitude	Altitude(km)	Event[a]	$t_{1/2}$ (UT)[b]	$H/v_\perp$(s)	ϵ(s$^{1/2}$)	$(v_\perp/H)^{1/2}\epsilon$	H(km)	T(K)[c]
KAO[d]	16° 36' 18.0"	-151° 41' 50.1"	13.555	I	14:28:15.11 ± 0.30	2.53	0.0079	0.0047	54.8	158
	17° 20' 07.3"	-148° 22' 50.1"	13.690	E	14:59:03.48 ± 0.32	2.97	0.0086	0.0050	64.0	184
MSO	-35° 19' 14.3"	-149° 00' 27.6"	0.767	I	14:27:04.87 ± 1.52[e]	2.76	0.0225	0.0135	64.9	187
AAT	-31° 16' 37.3"	-149° 03' 57.9"	1.165	I	14:27:06.62 ± 0.27	2.16	0.0021	0.0014	50.6	146
				E	15:00:27.22 ± 0.27	2.51	0.0019	0.0012	58.8	169
ANU	-31° 16' 22.0"	-149° 03' 39.4"	1.150	I	14:27:06.92 ± 0.57	2.53	0.0283	0.0178	59.3	171
				E	15:00:26.99 ± 1.07	2.66	0.0572	0.0351	62.3	179
IRTF	19° 49' 34.0"	155° 28' 15.0"	4.100	I	14:24:51.11 ± 0.29	2.70	0.0064	0.0039	58.9	170
				E	14:56:15.71 ± 0.84[f]	(2.70)[g]	0.0438	0.0267	----	---
UH	19° 49' 34.0"	155° 28' 20.0"	4.215	I	14:24:50.70 ± 0.33	2.40	0.0115	0.0074	52.4	151
				E	14:56:17.84 ± 1.84[f]	2.13	0.0224	0.0153	46.3	133

[a] I and E stand for immersion and emersion, respectively.
[b] Half-light times from isothermal fits to 200 s of data from 60^s above half-light to 140^s below half-light, except as noted. See text for discussion of uncertainties in the times.
[c] T/H = 2.88 K/km assumed.
[d] Summed data, with each channel weighted as ϵ^{-2}.
[e] The large timing uncertainty is due to uncertainties in the signal levels used for the color-correction technique applied to these observations. 100 s of data were used for the isothermal fit.
[f] Emersion occurred during dawn at Hawaii, resulting in large timing uncertainties.
[g] $H/v_\perp$ held fixed during isothermal fit.

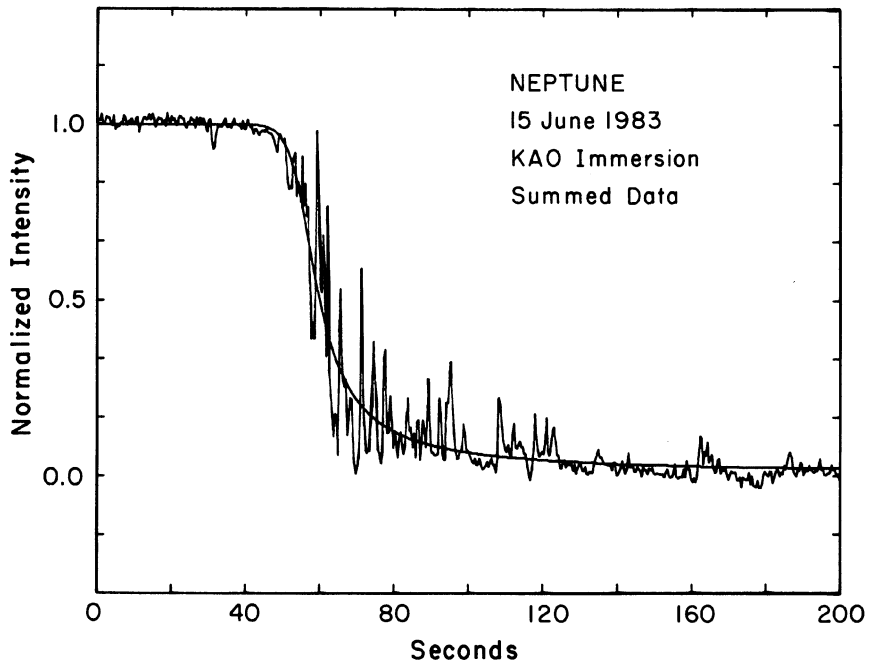

FIG. 1. Immersion event of 15 June 1983 observed from the *KAO*. The light curve represents the weighted sum of both channels of data, plotted at a resolution of 0.4. The best-fitting isothermal model curve is also shown. The time axis begins at 14:27:15 UT.

tively, where each channel was weighted by ϵ^{-2} prior to the summation. In these and subsequent figures, the smooth curve corresponds to the best-fitting isothermal model.

2) MSO

Immersion occurred during variable cloudiness, and emersion was clouded out. Since the event was observed at two wavelengths, and the occulted star was appreciably redder than the planet and sky background, it was possible to remove the effects of variable extinction almost completely.

We modeled the total signal $N(t)$ in each of two channels as

$$N_1(t) = n_{b_1} + [n_{p_1} + n_{*_1}\phi(t)]e^{-\tau(t)} \quad (4)$$

and

$$N_2(t) = n_{b_2} + [n_{p_2} + n_{*_2}\phi(t)]e^{-\tau(t)}, \quad (5)$$

where n_b represents a constant background signal level, the cloud is assumed to be a grey absorber of optical depth $\tau(t)$, and the terms in square brackets represent the planet (n_p) and star (n_*) contributions to the signal, in the absence of

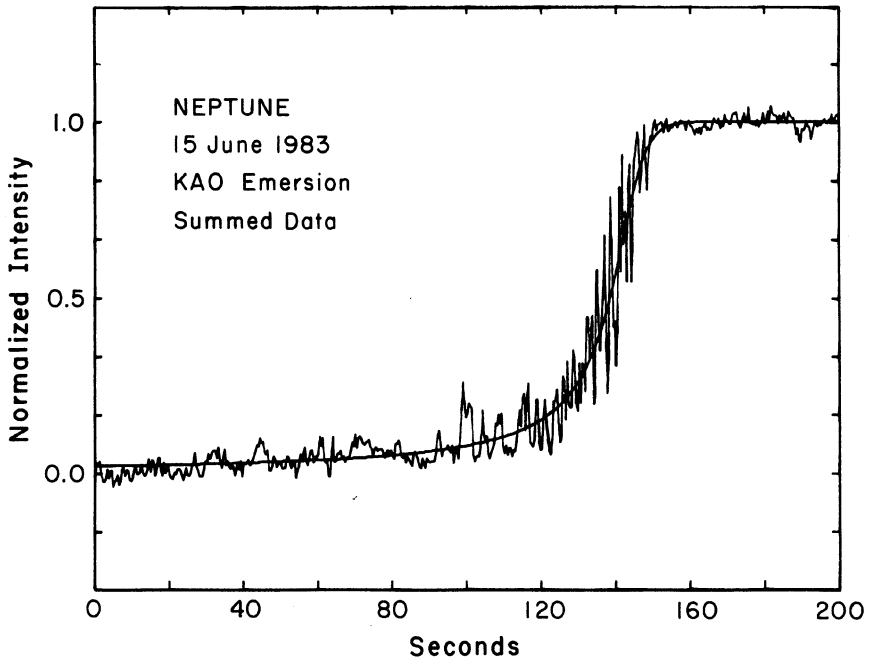

FIG. 2. Emersion event of 15 June 1983 observed from the *KAO*. The light curve represents the weighted sum of four channels of data, plotted at a resolution of 0.4. The best-fitting isothermal model curve is also shown. The time axis begins at 14:56:45 UT.

clouds. The signal from the star is modulated by refraction as it passes through the distant planetary atmosphere, and this is modeled as the normalized light curve $\phi(t)$, assumed to be wavelength independent. Solving for $\phi(t)$ from Eqs. (4) and (5), we find:

$$\phi(t) = \frac{n_{p_1}[N_2(t) - n_{b_2}] - n_{p_2}[N_1(t) - n_{b_1}]}{n_{*_2}[N_1(t) - n_{b_1}] - n_{*_1}[N_2(t) - n_{b_2}]} . \quad (6)$$

This color-correction technique is analogous to the method used by Elliot *et al.* (1975) to recover the light curve of the β Sco C occultation by Jupiter. The difference is that the present method assumes a constant background to correct for variable extinction, whereas Elliot *et al.*'s method assumed a constant extinction to correct for a variable background.

Equation (6) was used to determine $\phi(t)$ for the immersion Mount Stromlo data. The constants n_b, n_p, and n_* for each channel were determined by examining the light curves in regions where $\{\phi = 1, \tau = 0\}$, $\{\phi = 0, \tau = 0\}$ and $\{\tau = \infty\}$, although in principle these constants could have been determined by a simultaneous least-squares fit to data prior to the occultation and between immersion and emersion.

As an illustration of the effectiveness of this technique, Fig. 3 shows separate light curves for each channel during

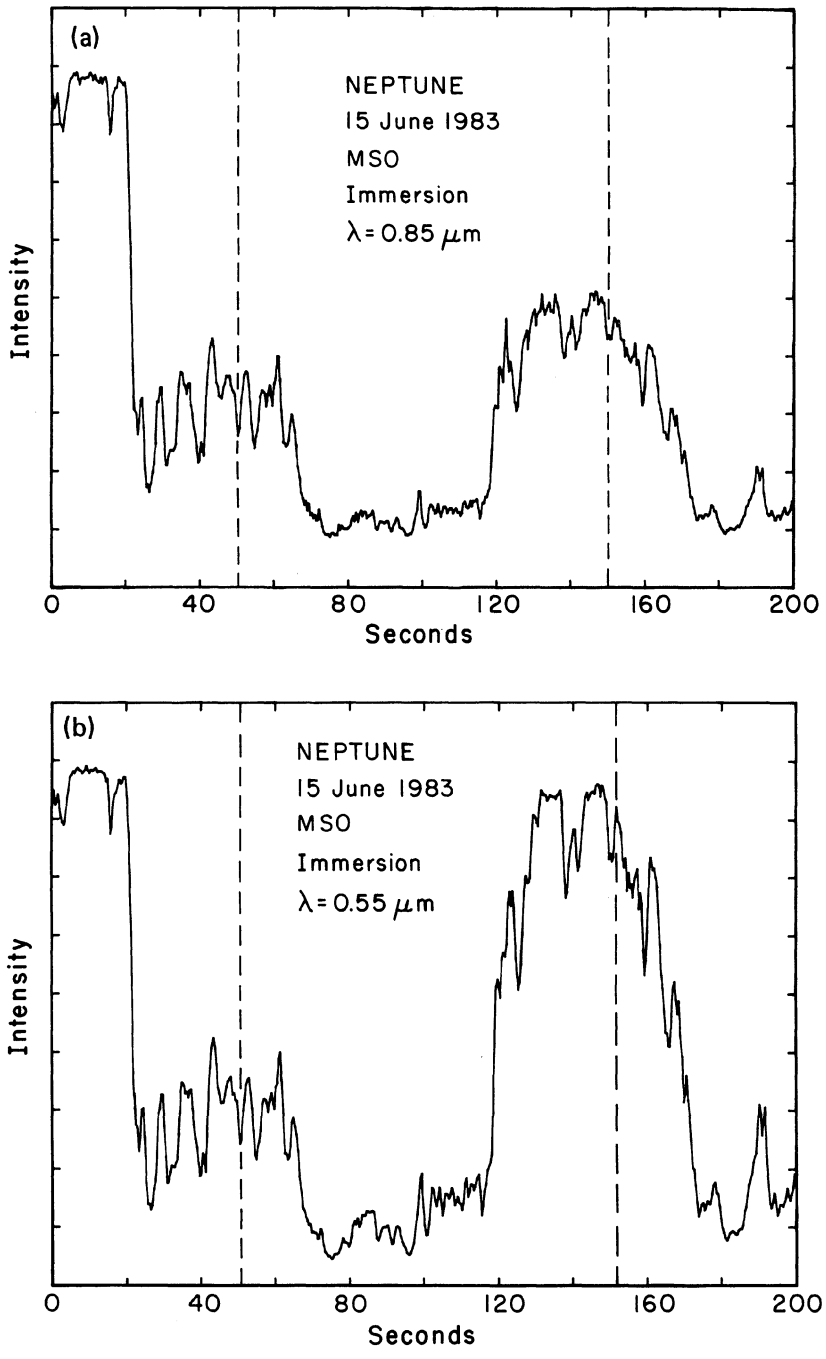

FIG. 3. Immersion event of 15 June 1983 observed from Mount Stromlo Observatory. The red and blue channels are shown in (a) and (b), respectively. Both channels show considerable variation due to intermittent cloudiness. However, since the star is relatively bright in the red channel and is faint in the blue channel, it is possible to remove the effects of variable extinction. The resulting light curve (c) corresponds to the 100 s interval between the vertical dashed lines in (a) and (b). The best-fitting isothermal model curve is also shown. All data are plotted at a resolution of 0.4. Time axes (a) and (b) begin at 14:25:40 UT. The time axis for (c) begins at 14:26:30 UT.

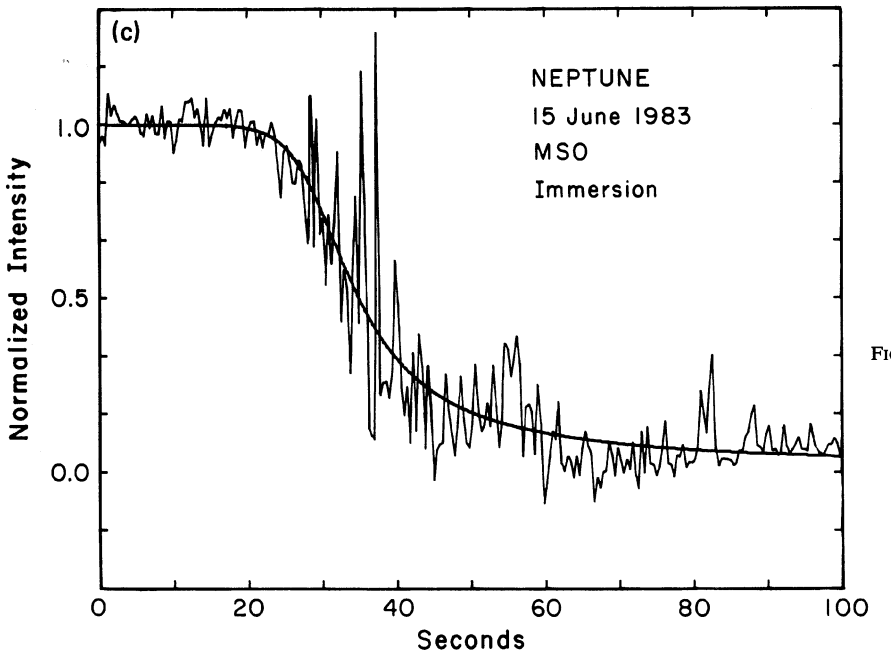

FIG. 3 (continued)

immersion. The variation in cloudiness completely dominates the light curve for each channel separately [Figs. 3(a) and 3(b)], but the reconstructed curve [Fig. 3(c)] contains almost no trace of these variations. However, the remaining large uncertainties in the zero and full stellar intensity levels are responsbile for the relatively poor precision of the half-light time (Table II). It is possible that there was a color-dependent component to the absorption by the clouds, or a variable background, not accounted for in the model.

3) AAT

Figures 4 and 5 show the immersion and emersion light curves obtained at the AAT. These observations have the lowest noise figure of the entire set (see Table II), and have extremely stable baselines as well. Variable cloudiness occurred during the observations, but was not significant during the immersion and emersion regions shown.

4) ANU

These two-color observations were corrected for variable cloudiness using the method described above [Eq. (6)]. However, the cloudiness was not so extreme as at Mount Stromlo, with $\tau(t) \ll 0.1$ throughout most of the occultation. The resulting curves are shown in Figs. 6 and 7.

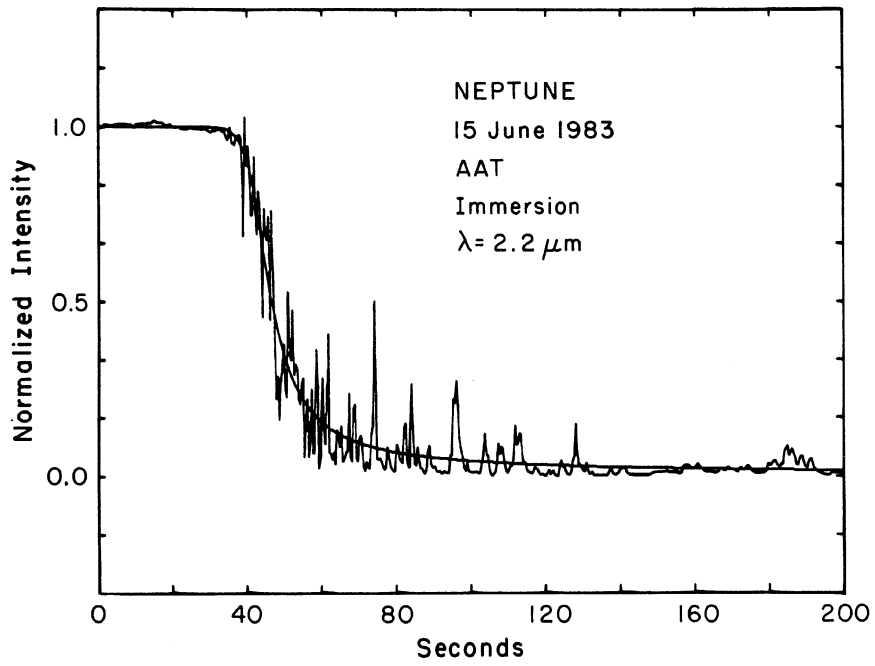

FIG. 4. Immersion event of 15 June 1983, observed from the AAT, plotted at a resolution of 0s4. The best-fitting isothermal model curve is also shown. Note the low noise level and the exceptionally flat baselines. The time axis begins at 14:26:19.998 UT.

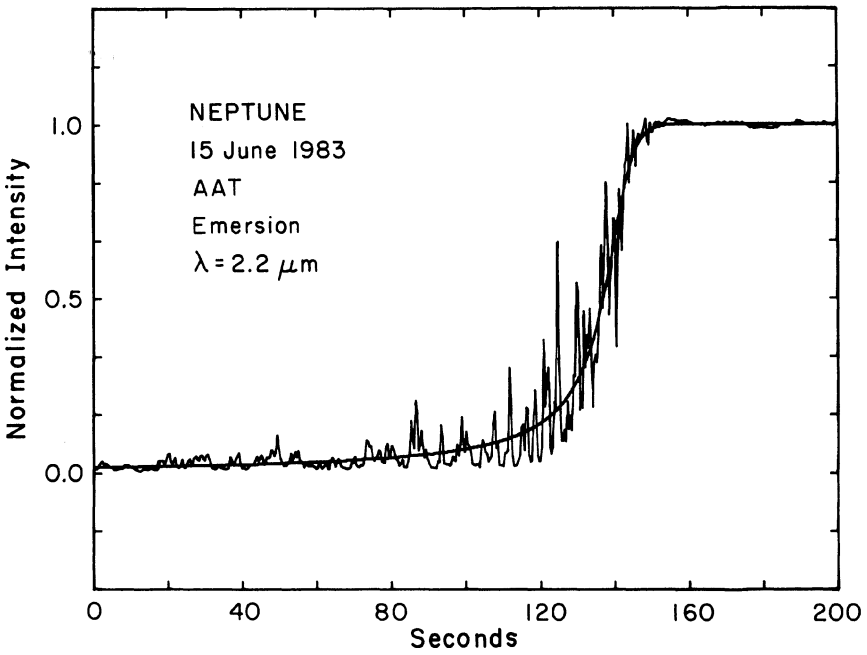

FIG. 5. Emersion event of 15 June 1983, observed from the AAT, plotted at a resolution of 0s4. The best-fitting isothermal model curve is also shown. Note the low noise level and the exceptionally flat baselines. The time axis begins at 14:58:09.998 UTC.

5) IRTF

The immersion observations (Fig. 8) have very stable baselines and a very low noise figure (Table II). However, emersion occurred during dawn, and the emersion light curve (Fig. 9) is considerably noisier, especially at post-emersion. This accounts for the large difference in the errors assigned to the immersion and emersion half-light times.

6) UH

Observing conditions at the UH telescope were similar to those at the IRTF, located on the same mountain. Immersion observations (Fig. 10) have stable baselines and low noise figure. Since the UH observations were made at 0.86 μm in an unchopped mode, the arrival of dawn is quite evident in the emersion light curve [Fig. 11(a)]. Both immersion and emersion curves were corrected for dead time by solving iteratively for the true counting rate N from the apparent counting rate M, where

$$M = Ne^{-N\rho} \tag{7}$$

and ρ is the resolving time of the detector, measured to be 4.5×10^{-7} s. The data have also been corrected for a slow drift in the system clock. (This correction amounted to less

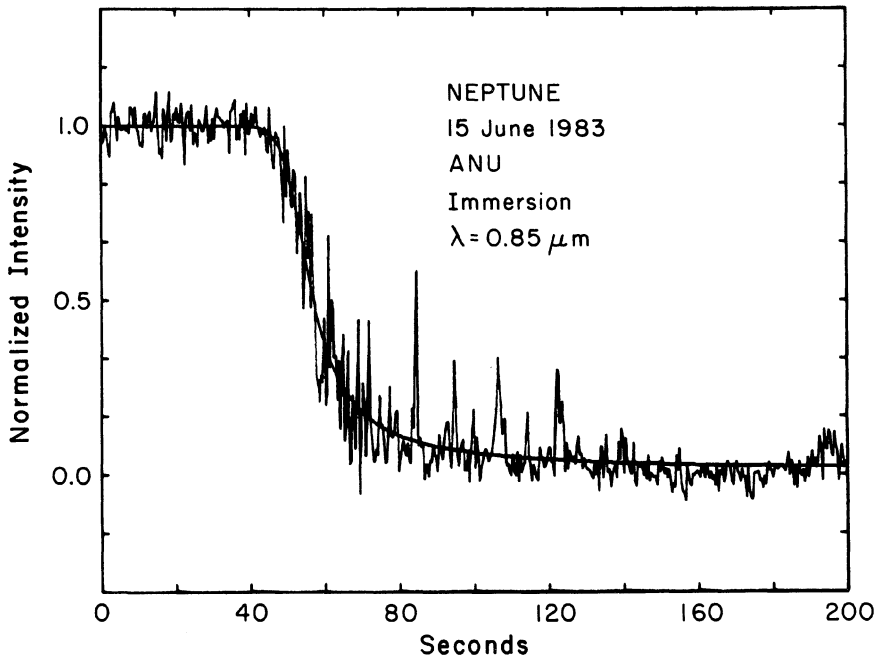

FIG. 6. Immersion event of 15 June 1983, observed from ANU, plotted at a resolution of 0s4. The best-fitting isothermal model curve is also shown. The data have been corrected for variable cloudiness. See the text for details. The time axis begins at 14:26:09.981 UTC.

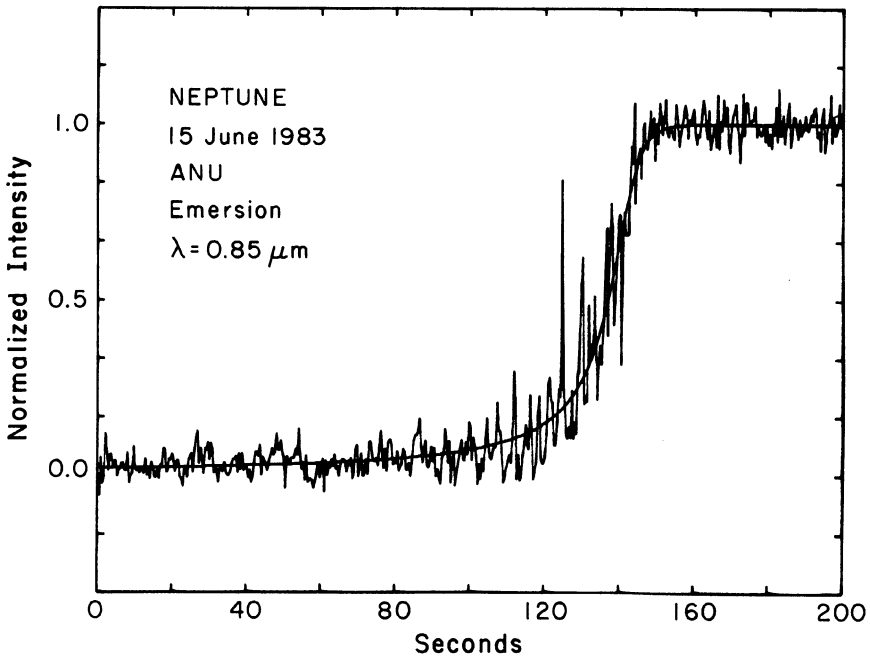

FIG. 7. Emersion event of 15 June 1983, observed from ANU, plotted at a resolution of 0s4. The best-fitting isothermal model curve is also shown. The data have been corrected for variable cloudiness. See the text for details. The time axis begins at 14:58:09.981 UTC.

than 0s07, far less than the uncertainty in the half-light times.)

The time-varying dawn contribution was removed from the emersion curve as follows. Prior to emersion, where $\phi(t) \simeq 0$, the signal was modeled as

$$\text{pre-emersion: } N = a + bt + ct^2. \quad (8)$$

After emersion, where $\phi(t) = 1$, the signal was modeled as

$$\text{post-emersion: } N = n_* + a + bt + ct^2. \quad (9)$$

A linear least-squares solution was obtained for the constants a, b, and c, and n_*, the signal from the unocculted star, was estimated by an isothermal fit to the resulting dawn-corrected curve. The procedure was repeated until self-consistent values of all four constants were obtained. This required just two iterations. The model dawn curve is shown in Fig. 11(a), and the dawn-corrected curve is shown in Fig. 11(b), with the best-fitting isothermal model curve.

b) 7 April 1968 Event Timing

We have included the 1968 occultation events in our solution for the size and oblateness of Neptune, using the event times given by Kovalevsky and Link (1969), and tabulated in

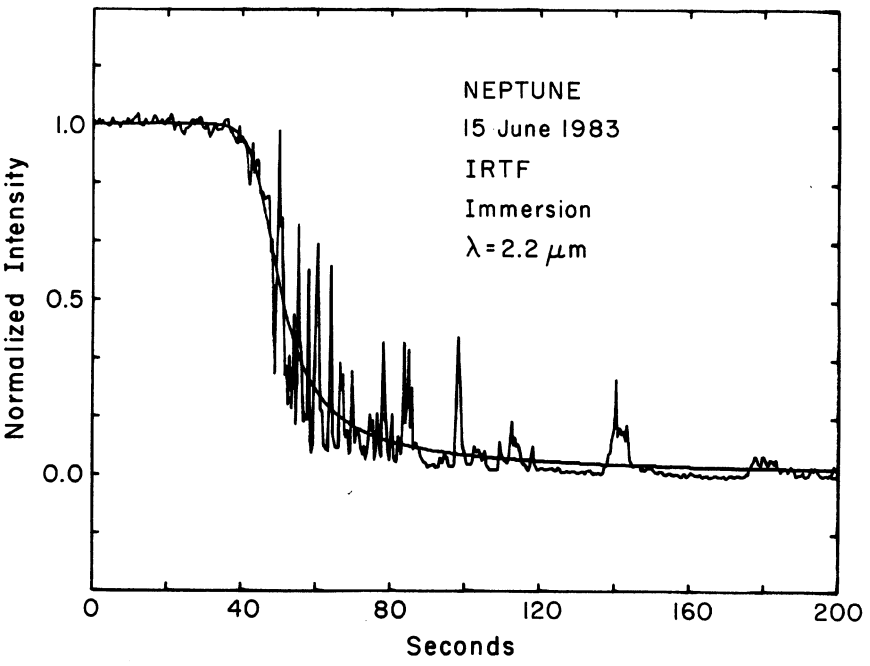

FIG. 8. Immersion event of 15 June 1983, observed from the IRTF, plotted at a resolution of 0s4. The best-fitting isothermal model curve is also shown. The time axis begins at 14:24:00 UTC.

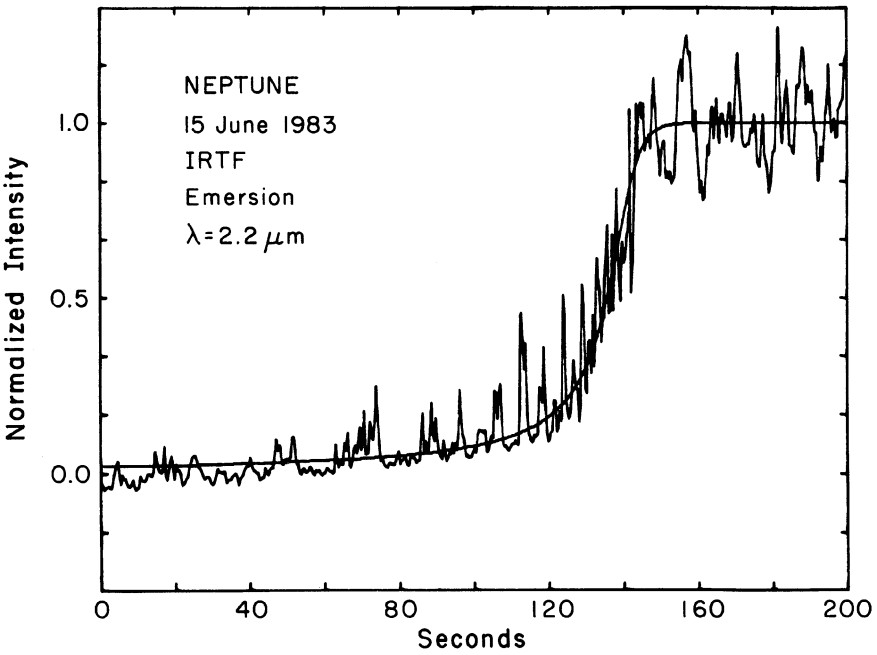

FIG. 9. Emersion event of 15 June 1983, observed from the IRTF, plotted at a resolution of 0s.4. The noise level is considerably greater than the immersion noise level (Fig. 8), since the emersion event occurred during dawn. The best-fitting isothermal model curve is also shown. The time axis begins at 14:53:59 UTC.

Table III. These observations were recorded on strip charts and were later digitized, a potential source of considerable error in the derived half-light times, due to the difficulty of digitizing a slow-speed chart record, possible uneven chart speeds, and uncertainties in absolute timing. The errors assigned to the half-light times given in Table III were estimated as follows. For the Dodaira and Okayama observations, the half-light times quoted by Kovalevsky and Link (1969) are *not* based on isothermal fits, as can be seen by examining their Fig. 3. We digitized the facsimiles of the Japanese observations given by Kovalevsky and Link, and obtained half-light times by fitting isothermal models to the resulting curves. We performed this entire operation twice for each curve, and the differences in the derived half-light times so obtained are adopted as estimates of the uncertainty in the half-light times. Our half-light times are in reasonable agreement with Kovalevsky and Link's values. For the Mount Stromlo (MSO) data, which were recorded on a very compressed scale, we have adopted Freeman and Lyngå's (1970) estimate of $\pm$ 2 s as the uncertainty in the half-light time.

III. DATA ANALYSIS

a) Solving for the Oblateness

We used the method described by French and Taylor (1981) to determine the planetary oblateness and equatorial

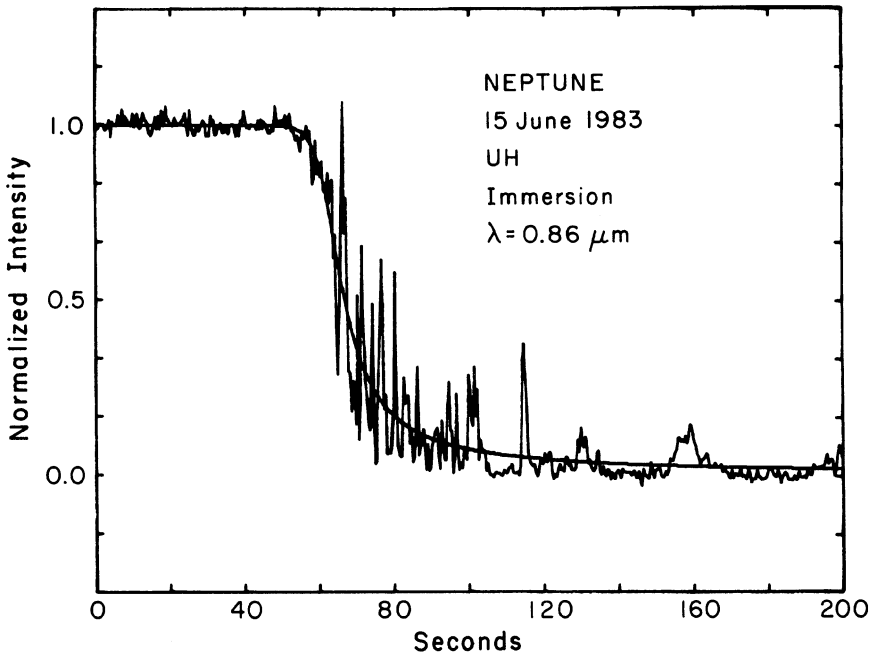

FIG. 10. Immersion event of 15 June 1983, observed from UH, plotted at a resolution of 0s.4. The best-fitting isothermal model curve is also shown. The data have been corrected for dead time. The time axis begins at 14:23:43:832 UTC.

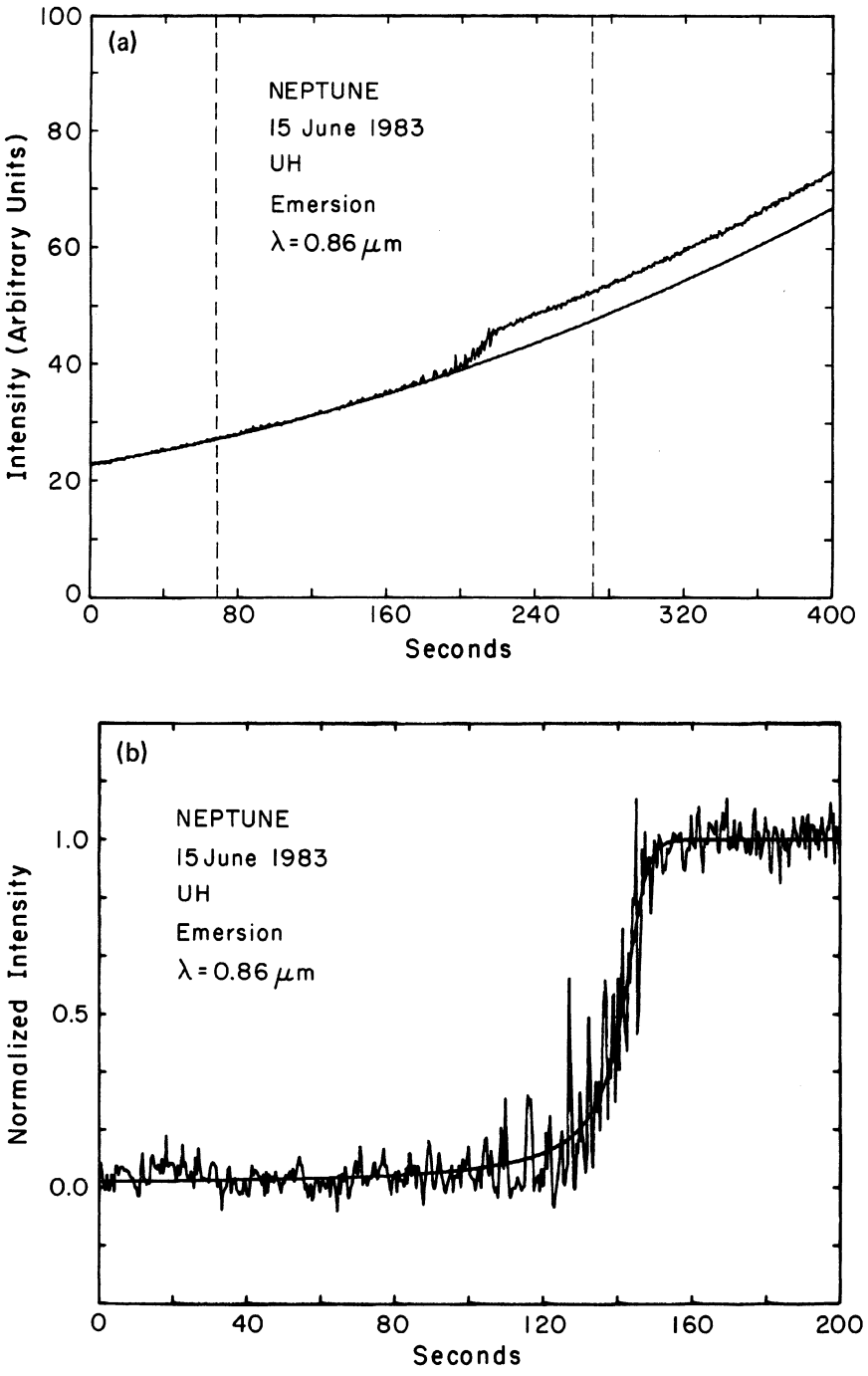

FIG. 11. Emersion event of 15 June 1983, observed from UH, plotted at a resolution of 0s.4. The arrival of dawn is clearly evident in (a), where the smooth curve represents a model of the increasing sky brightness due to approaching sunrise. In (b), the sky-brightness model has been subtracted from the data, for the 200 s interval between the vertical dashed lines in (a). The best-fitting isothermal model curve is also shown. The data have been corrected for dead time. The time axis for (a) begins at 14:52:46.654 UTC and for (b) begins at 14:53:56.654 UTC.

radius. First, we computed the coordinates of the observer in the fundamental plane for the set of half-light times and observatory positions. The assumed center of Neptune was computed using the DE-96 ephemeris (Standish *et al.* 1976). Next, we fitted ellipses to the set of half-light points in the fundamental plane for the 1968 and 1983 observations, where the ellipses were defined by the orientation of Neptune's pole at the time of each occultation, and by the oblateness and equatorial radius of the planet. (To first order in the oblateness, an ellipse is an accurate representation of the projection of the figure of an axially symmetric slowly rotating planet.) The occultation chords used in the fit are shown in Figs. 12 and 13 for the 1968 and 1983 events, respectively. The stellar occultation by Neptune of 24 May 1981 (French *et al.* 1983a) was not used in the fit, because half-light times were available from only one station. These two additional data points provide the degrees of freedom necessary to determine the relative positions of the planet and the occulted star, but they do not provide any information about Neptune's radius and oblateness. We adopted Harris' (1984) description of Neptune's pole, with the position angles P and declinations of the Earth B given in Table IV.

TABLE III. Event times for 7 April 1968 observations.

Station	Latitude	Longtitude	Altitude(km)	Event[a]	$t_{1/2}$ (UT)[b]
Dodaira	36° 00' 10.2"	-139° 11' 46.8"	0.879	I	15:56:25.5 ± 1.3
				E	16:41:28.0 ± 1.0
Okayama	34° 34' 22.8"	-133° 35' 46.6"	0.365	I	15:56:55.5 ± 1.2
				E	16:41:51.5 ± 1.0
MSO	-35° 19' 19.7"	-149° 00' 20.4"	0.770	I	15:56:29 ± 2
				E	16:36:46: ± 2

(a) I and E stand for immersion and emersion, respectively.

(b) Event times are taken from Kovalevsky and Link (1969). See text for discussion of assigned errors in half-light times.

The quantities determined by the least-squares fit are r_e, the equatorial radius, f, the oblateness (defined by $f = 1 - r_p/r_e$, where r_p is the polar radius), and corrections to the Neptune ephemeris for both occultations. Since the true independent variable is the half-light time, the fit minimized the sum of squared residuals in time, rather than in radial distance. (However, our results are essentially unchanged when the sum of squared radius residuals is minimized instead.) Gravitational and refractive bending were also taken into account. The correction in r_e due to general relativity is of order

$$\Delta r_{gr} = 4GMD/r_e c^2 \approx 50 \text{ km}, \quad (10)$$

where G is the gravitational constant, M is the mass of Neptune (Standish and Campbell 1984), D is the Earth-Neptune distance, and c is the velocity of light. The correction in r_e due to refractive bending of a half-light ray is $\Delta r_{rb} = H$. We adopted $\Delta r_{rb} = 50$ km, equal to the general relativistic correction, for all observations.

The results of our weighted fit to the data in Tables II and III are given in Tables V and VI. Table V includes, for each data point, the sky-plane coordinates, the perpendicular velocity $v_\perp$, the Neptune suboccultation latitude θ, the residuals of the fit in time (Δt) and radius (Δr), and the time residual normalized by the adopted half-light time uncertainty $\sigma(t_{1/2})$, as given in Tables II and III. $|\Delta t/\sigma(t_{1/2})|$ provides a comparative measure of the goodness of fit to each data point. Table VI contains the final values of the fitted parameters and their formal errors.

Our adopted oblateness of $f = 0.0191 \pm 0.0017$ for the joint fit to the 1968 and 1983 observations is smaller than, but consistent with, Kovalevsky and Link's (1969) result of $f = 0.021 \pm 0.004$. As a check, we fitted the 1968 data alone, using Kovalevsky and Link's adopted pole position and planetary ephemeris, and we reproduced their results. Since the 1968 observations have relatively large timing uncertainties, they have less leverage than the 1983 observations on the results of the weighted joint fit. The planetary radius determined from the fit, 25 268 ± 12 km, is comparable to Kovalevsky and Link's (1969) value of 25 225 ± 30 km, Freeman and Lyngå's (1970) value of 25 265 ± 36 km, and Hubbard *et al.*'s (1985) result of 25 295 ± 50 km.

In principle, the orientation of Neptune's pole at a given epoch could be determined from the joint observations, in much the same way as the pole of Uranus is determined from multiple ring occultations (Elliot *et al.* 1981). Unfortunately, the orientation of Neptune in 1968 and 1983 (see Figs. 12 and 13) was not favorable for such a solution because of the small values of B, the declination of the Earth (see Table IV). We obtained results consistent with Harris' (1984) values, but the formal uncertainties in the right ascension and declination of the pole were rather large ($\sim \pm 5°$).

We performed several fits to determine the sensitivity of our results to a change in pole direction. The results are

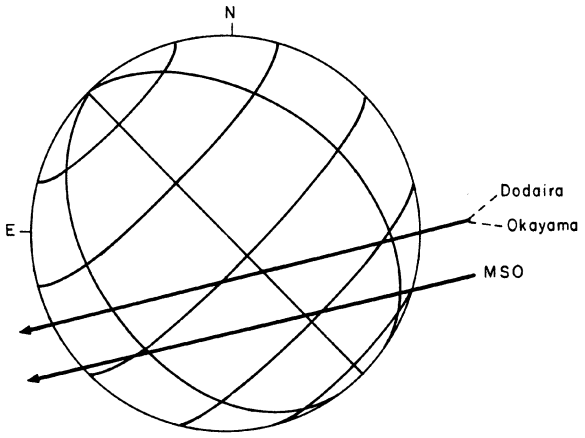

FIG. 12. Occultation chords across Neptune for the 7 April 1968 event.

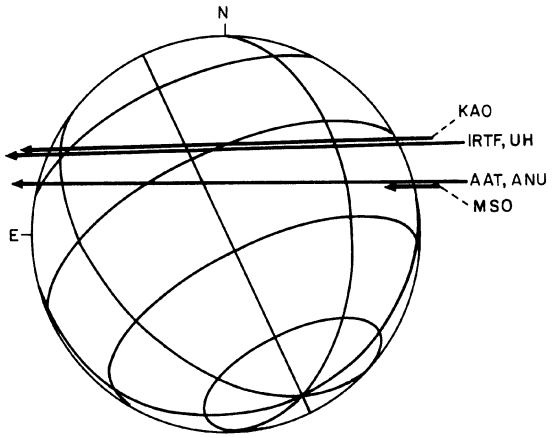

FIG. 13. Occultation chords across Neptune for the 15 June 1983 event.

TABLE IV. Assumed orientation of Neptune's pole.[a]

Date	B	P
7 April 1968	9.47°	45.17°
15 June 1983	-23.95°	25.26°

[a] Based on Harris (1984), assuming Alden's (1943) value for the mass of Triton.

summarized below:

$$dr_e/d\alpha_p = +3.9 \text{ km deg}^{-1},$$
$$dr_e/d\delta_p = -3.5 \text{ km deg}^{-1},$$
$$d(\ln f)/d\alpha_p = -0.025 \text{ deg}^{-1},$$
$$d(\ln f)/d\delta_p = +0.005 \text{ deg}^{-1}. \quad (11)$$

b) Temperature Profiles of Neptune's Upper Atmosphere

Neptune's upper atmospheric thermal structure can be obtained from stellar occultation observations by numerical inversion, subject to well-known assumptions (French *et al.* 1978). We inverted the highest-quality observations from the 15 June 1983 occultation, and obtained the immersion and emersion temperature profiles shown in Figs. 14 and 15, respectively. Because of the nature of the inversion method, the overall placement of the temperature profiles is uncertain by about $\pm$ 10 K. We adopted a mean molecular weight of 2.2 g mole^{-1}, a gravitational acceleration of 1090 cm s^{-2}, an atmospheric refractivity at STP of 1.26×10^{-4}, and a composition of 90% H_2, 10% He by number when performing the inversions. The range of altitude covered by the profiles is about 30 km above the level corresponding to the half-light time, to 200 km below the half-light level. Outside of the interval, the results are significantly influenced by the initial condition of the inversion and by uncertainties in the baseline levels of the light curves.

French *et al.* (1983a) obtained comparable profiles from the stellar occultation by Neptune of 24 May 1981. They found that immersion and emersion profiles were remarkably similar in overall shape, suggestive of global atmospheric layering. The present observations do not show any evidence of such layering. The mean temperatures of the profiles in Figs. 14 and 15 are comparable to the mean values obtained from the isothermal fits, which are 159 $\pm$ 6 K and 170 $\pm$ 15 K for the inverted immersion and emersion data, respectively. For comparison, Hubbard *et al.* (1985) obtained a mean temperature of 156 $\pm$ 10 K from their observations of this event. There is no evident latitude dependence in the mean temperatures, nor is there any evidence that the mean upper-atmospheric temperature is changing with time, as appears to be the case for Uranus (French *et al.* 1983b).

TABLE V. Astrometry data.

ASTROMETRY OF 7 APRIL 1968 EVENT
Sky Plane Coordinates[a]

Station	Event[b]	East(km)	North(km)	$v_\perp$(kms^{-1})	θ(°)	Δt(s)	$\lvert\Delta t\rvert/\sigma(t_{1/2})$	Δr(km)
Dodaira	I	-41323.3	1184.5	-17.55	-42.8	-0.02	0.02	0.4
	E	5800.3	-11273.6	17.59	17.1	-0.73	0.73	-12.9
Okayama	I	-41305.8	889.1	-17.49	-43.4	1.05	0.81	-18.4
	E	5693.2	-11509.2	17.54	16.5	0.06	0.06	1.0
MSO	I	-40416.7	-5801.2	-15.71	-58.5	-0.96	0.48	15.1
	E	1760.0	-16986.2	15.80	1.3	1.22	0.61	19.3

ASTROMETRY OF 15 JUNE 1983 EVENT
Sky Plane Coordinates[a]

Station	Event[b]	East(km)	North(km)	$v_\perp$(kms^{-1})	θ(°)	Δt(s)	$\lvert\Delta t\rvert/\sigma(t_{1/2})$	Δr(km)
KAO	I	-27220.2	7142.4	-21.62[c]	2.3	-0.39	1.29	8.4
	E	17284.7	6645.5	21.52[c]	46.1	0.00	0.01	0.0
MSO	I	-29232.8	1745.8	-23.50	-9.7	2.30	1.51	-54.1
AAT	I	-29179.3	2185.1	-23.41	-8.8	-0.26	0.95	6.1
	E	19279.9	1571.8	23.39	35.6	0.06	0.20	1.4
ANU	I	-29172.5	2185.5	-23.41	-8.8	0.02	0.03	-0.4
	E	19273.8	1572.4	23.39	35.6	-0.19	0.17	-4.1
IRTF	I	-27542.6	6467.6	-21.81	0.8	0.48	1.64	-10.5
	E	17771.0	5647.1	21.72	44.0	-0.42	0.50	-9.1
UH	I	-27552.5	6467.9	-21.81	0.7	0.07	0.20	-1.5
	E	17822.2	5646.3	21.72	44.0	1.70	0.93	36.9

[a] Computed using the DE-96 ephemeris for Neptune and star positions as given in Table VI.

[b] I and E stand for immersion and emersion, respectively.

[c] Uncorrected for velocity of the aircraft.

TABLE VI. Results of joint fit to 7 April 1968 and 15 June 1983 observations.

(a) Neptune Dimensions

Oblateness	0.0191 ± 0.0017	Equatorial Radius	25268 ± 12 km

(b) Differences between Perth 70 and DE-96 Reference Systems

Date	Time(UT)	Star	1950.0 Stellar Coordinates α	1950.0 Stellar Coordinates δ	Center of Neptune (Fit - DE-96) East(km)	Center of Neptune (Fit - DE-96) North(km)	Δ α	Δ δ
7 April 1968	16:00	BD-17°4388	$15^h35^m50^s.462$	-17°30'07".94	-16395 ± 21	467 ± 48	$-0^s.05353 \pm 0^s.00007$	0".0218 ± 0".0004
15 June 1983	14:45	MKE 30	$17^h49^m12^s.291$	-22°08'59".78	-4949 ± 10	-4591 ± 28	$-0^s.01679 \pm 0^s.00003$	-0".2164 ± 0".0013

IV. DISCUSSION

The oblateness of a planet is closely related to its rotation rate and gravitational field by (Stacey 1969)

$$f = 3J_2/2 + \omega^2 r_e^3/2GM \quad (12)$$

to first order in f and J_2, where ω is the rotation frequency, J_2 is the coefficient of the second harmonic of the gravitational potential, and the other terms have been defined previously. In principle, if any two of the quantities ω, f, and J_2 are known, the third can be inferred. A derived quantity of importance to planetary interior models is Λ_2, the second-degree response coefficient, defined as (Hubbard 1984)

$$\Lambda_2 \simeq J_2\, GM/\omega^2 r_e^3, \quad (13)$$

assuming that r_e is the reference radius for J_2. Λ_2 is a measure of the degree of central condensation: the smaller the value of Λ_2, the more centrally condensed is the planet.

Our first task is to determine if the current estimates for ω, J_2, and f are mutually consistent. We will argue that this is indeed the case, and we will then evaluate Λ_2 and investigate the implications for the internal structure of Neptune.

Belton and Terrile (1984) have reviewed recent work bearing on the rotational properties of Neptune, determined from the motions of spots in images of the planet and extended time series of photometric observations. We adopt Belton *et al.*'s (1981) recommended period of 18.2 ± 0.4 hr. The assigned uncertainty is based on the inferred presence of significant ($\sim$100 m s^{-1}) zonal winds on Neptune. Harris (1984) reanalyzed the motion of Triton and found that $J_2 = 0.0043 \pm 0.003$ if Triton's mass is 1.28×10^{-3} times Neptune's mass, as given by Alden (1943), and $J_2 = 0.0037 \pm 0.0002$ if Triton is much less massive. (Harris assumed a rotational period of 18.2 hr when deriving these results, consistent with Belton *et al.*'s recommended value).

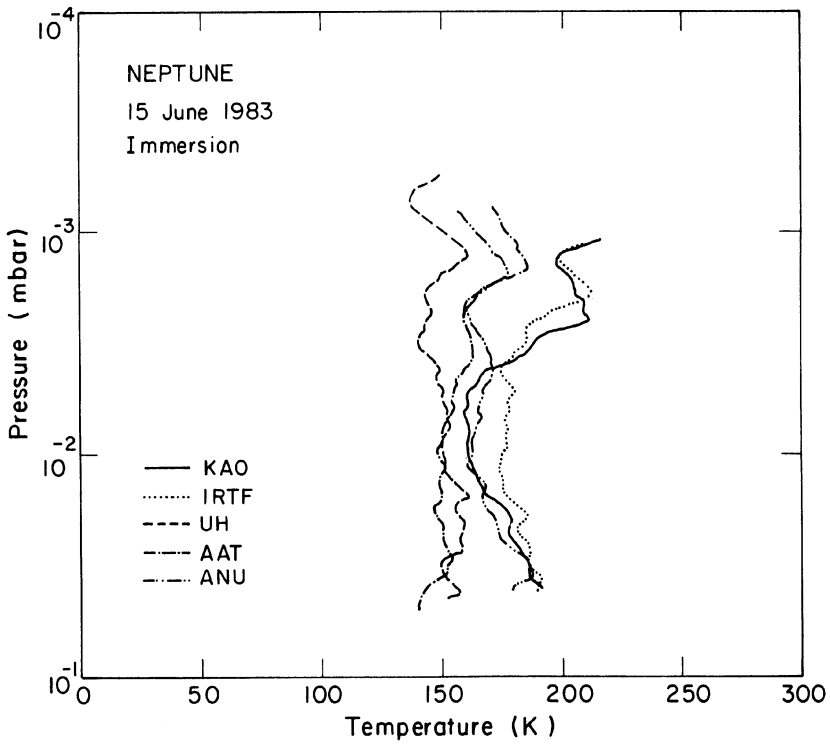

FIG. 14. Temperature profiles obtained by inversion of immersion light curves for the 15 June 1983 event.

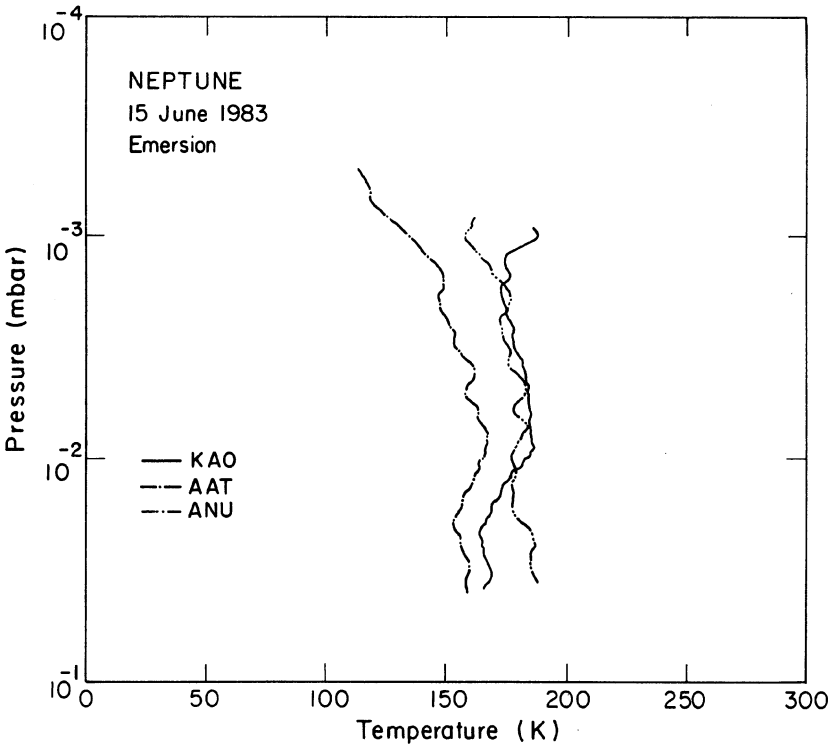

FIG. 15. Temperature profiles obtained by inversion of emersion light curves for the 15 June 1983 event.

This poses a challenge to our theoretical understanding of Neptune's interior, since all existing models predict a greater degree of central condensation than the observations suggest (see Hubbard and McFarlane 1980; and Hubbard 1984, and references cited therein).

From Harris' (1984) analysis, it is possible to determine self-consistent combinations of Neptune's rotation period, the ratio of Triton's mass to Neptune's (M_T/M_N), and oblateness. This is done by equating the components of Triton's orbital angular momentum and Neptune's spin angular momentum, which lie in the invariable plane, and using the Darwin-Radau relation.

Figure 16 shows the range of mass ratios (M_T/M_N) and rotation periods that are consistent with our oblateness determinations. For completeness, we have considered both direct and retrograde rotation of Neptune. The bold solid line corresponds to direct rotation with $f = 0.0191$, our nominal solution. The corresponding case for retrograde rotation is shown dashed. Since the inclination of Triton's orbit is uncertain by $\pm$ 1.5° (Harris 1984), there is a corresponding uncertainty in the overall position of these curves, shown by the dotted region. Also shown are solutions for $f = 0.0174$ and $f = 0.0208$, corresponding to one standard deviation below and above the nominal value. The dot and error bar mark the range of direct rotation periods consistent with Alden's mass for Triton. We find $P = 16.9 \pm 1.2$ hr, consistent with, but somewhat shorter than, Belton *et al.*'s choice of 18.2 hr.

We can also evaluate Λ_2 and compare our results to Λ_2 for the other giant planets. The results are shown in Fig. 17, where Λ_2 is plotted versus rotation period for the same range of oblateness as Fig. 16. The dashed region is bounded from the left and right by the formal errors on our oblateness determination, from above by assuming that Alden's mass for Triton represents a reasonable upper limit to the true value, and from below by assuming Neptune's rotation is direct. The dot corresponds to the nominal solution for the oblateness and Alden's mass for Triton. Λ_2 for Jupiter, Saturn, and Uranus (Hubbard 1984), marked by J, S, and U, are shown for comparison. For *all* direct rotation solutions, we find

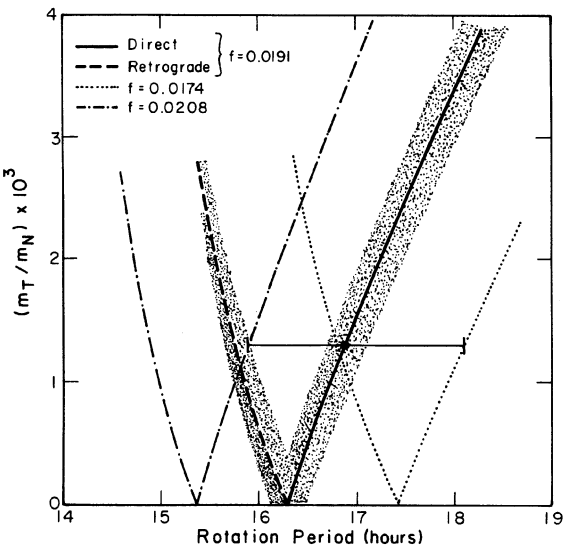

FIG. 16. Ratio of Triton's to Neptune's mass (M_T/M_N), as a function of Neptune's rotation period, for the range of oblateness $f = 0.0191 \pm 0.0017$. Both direct and retrograde rotations are shown. The dot and error bar mark the range of rotation periods consistent with our oblateness determination and Alden's (1943) mass of Triton. The dotted strips show the uncertainty in the position of a typical curve due to the uncertainty in the inclination of Triton's orbit.

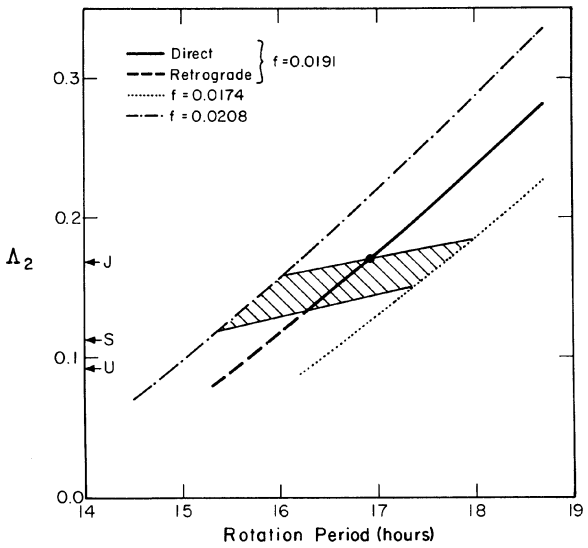

FIG. 17. The second-order response coefficient Λ_2 as a function of Neptune's rotation period, for the range of oblatenesses $f = 0.0191 \pm 0.0017$. Both direct and retrograde rotations are shown. The dot corresponds to the nominal solution for f and Alden's (1943) result for the mass of Triton. The hatched region is delimited to the left and right by our oblateness solution, from above by assuming that Alden's mass for Triton is an upper limit, and from below by assuming that Neptune's rotation is direct. Λ_2 for Jupiter (J), Saturn (S), and Uranus (U) are also shown.

that Neptune's Λ_2 is significantly different from Uranus' and is much closer to that of Jupiter. In fact, if we adopt the nominal values of P and (M_T/M_N), Neptune is *the least centrally condensed of all the giant planets*, a conclusion reached by Dermott (1984) using a related argument.

Our findings differ in several important respects from Hubbard *et al.*'s (1985) analysis of independent observations of the 15 June 1983 occultation. They obtained an oblateness of $f = 0.022 \pm 0.004$, consistent with our result, and inferred a rotation period $P = 15^h(+3^h, -2^h)$, from which they concluded that Neptune and Uranus may have homologous mass distributions. This conclusion depends critically on the rejection of Belton *et al.*'s (1981) 18.2 hr rotation period. As Hubbard (1984) pointed out, "if Neptune's rotation period were taken to be equal to 18^h or greater, the corresponding Λ_2 for Neptune would equal 0.20 or greater, making this planet's interior structure grossly dissimilar to that of Uranus or any other Jovian planet." Hubbard *et al.* (1985) adopt a shorter period on the basis of their larger oblateness. The quoted uncertainty in their oblateness is greater than ours. (We suspect this is because they used only five data points to derive four free parameters, because the noise figure $(v_\perp/H)^{1/2}\epsilon$ was large for several of their data points, and because the 1968 observations were not included in their fit.) If one ignores the independent observations that support a rotation period of order 18 hr, then a key to demonstrating the nonhomology of Uranus and Neptune is the relatively small error bars we have obtained for the oblateness. As discussed in Sec. II*a*, the error is dominated by the formal error of the fit; a systematic error in the pole direction as large as 3° would change the oblateness by less than the quoted error [Eq. (11)]. Of greater concern is the possibility for systematic errors in the event times derived from the light curves due to terrestrial atmospheric turbulence, passing clouds, and inaccurate time keeping. Unfortunately, it is difficult to track down such errors. There remains the possibility of an improved fit by combining our results with Hubbard *et al.*'s. This would require some care. Ideally, the same fitting procedure should be used for all data sets to obtain the half-light times.

In our view, Belton *et al.*'s (1981) 18.2 hr rotation period, Harris' (1984) nominal value for J_2, and our measured oblateness comprise a mutually consistent set, and support the conclusions that Neptune and Uranus are significantly different, and that interior models for Neptune need to be improved.

V. CONCLUSIONS

From a joint analysis of the 7 April 1968 occultation of BD − 17°4388 and the 15 June 1983 occultation of MKE 30, we have determined improved values for the radius and oblateness of Neptune. The oblateness so determined is consistent with recent redeterminations of J_2 and the planet's rotation period, which provides support for the accuracy of all three measurements. Using these results, we conclude that Neptune's interior is far less centrally condensed than Uranus', a difference not yet accounted for in theoretical models. Additional occultation observations should allow the oblateness to be determined with even greater precision.

We would like to thank the staff of the *Kuiper Airborne Observatory* and the support staff of the UH for assistance with the observations. This work was supported in part by NASA Grants Nos. NSG-2342 and NGL 12-001-057, by NSF Grant No. AST 8209825, and by a grant from the National Geographic Society.

REFERENCES

Alden, H. L. (1943). Astron. J. **50**, 110.
Belton, J. J. S., and Terrile R. (1984). Proceedings of the Uranus and Neptune Workshop, Pasadena, CA, February 6–8, 1984.
Belton, J. J. S., Wallace, L., and Howard S. (1981). Icarus **46**, 263.
Dermott, S. F. (1984). Philos. Trans. R. Soc. London A **313**, 123.
Elliot, J. L. (1979). Annu. Rev. Astron. Astrophys. **17**, 445.
Elliot, J. L., Allen, D. A., Ashley, M. C. B., Baron, R. L., Dunham, E., Erickson, E. F., Freeman, K. C., French, R. G., Goguen, J. D., Hammel, H. B., Meech, K. J., and Mink, D. J. (1985). Astron. J. **90**, 2615 (Paper I).
Elliot, J. L., Dunham, E., Mink, D. J., and Churms, J. (1980). Astrophys. J. **236**, 1026.
Elliot, J. L., French, R. G., Frogel, J. A., Elias, J. H., Mink, D. M., and Liller, W. (1981). Astron. J. **86**, 444.
Elliot, J. L., Wasserman, L. H., Veverka, J., Sagan, C., and Liller, W. (1975). Astron. J. **80**, 323.
Freeman, K. C., and Lyngå, G. (1970). Astrophys. J. **160**, 767.
French, R. G., Elias, J. H., Mink, D. J., and Elliot, J. L. (1983a). Icarus **55**, 332.
French, R. G., Elliot, J. L., Dunham, E. W., Allen, D., Elias, J. H., Frogel, J. A., and Liller W. (1983b). Icarus **53**, 399.
French, R. G., Elliot, J. L., and Gierasch, P. J.(1978). Icarus **33**, 186.
French, R. G., and Taylor, G. E. (1981). Icarus **45**, 577.

Harris, A. W. (1984). Proceedings of the Uranus and Neptune Workshop, Pasadena, CA, February 6–8, 1984.
Hubbard, W. B. (1984). Proceedings of the Uranus and Neptune Workshop, Pasadena, CA, February 6–8, 1984.
Hubbard, W. B., Frecker, J. E., Gehrels, J. A., Gehrels, T., Hunten, D. M., Lebofsky, L. A., Smith, B. A., Tholen, D. J., Vilas, F., Zellner, B., Avey, H. P., Mottram, K., Murphy, T., Varnes, B., Carter, B., Nielsen, A., Page, A. A., Fu, H. H., Wu, H. H., Kennedy, H. D., Waterworth, M. D.,and Reitsema, H. J. (1985). Astron. J. **90**, 655.
Hubbard, W. B., and MacFarlane, J. J. (1980). J. Geophys. Res. **85**, 225.
Kovalevsky, J., and Link, F. (1969). Astron. Astrophys. **2**, 398.
Melroy, P. A. (1984). Master's thesis, Massachusetts Institute of Technology.
Mink, D. J., Klemola, A. R., and Elliot, J. L. (1981). Astron. J. **86**, 135.
Stacey, F. D. (1969). *Physics of the Earth* (Wiley, New York).
Standish, E. M., and Campbell, J. K. (1984). Bull. Am. Astron. Soc. **16**, 722.
Standish, E. M., Keesey, J. S. W., and Newhall, X X (1976). JPL Technical Report 32-1603.